ACS APPLIED MATERIALS & INTERFACES

Research Article

www.acsami.org

Ionic Liquid-Assisted Synthesis of Pt Nanoparticles onto Exfoliated Graphite Nanoplatelets for Fuel Cells

Inhwan Do[†] and Lawrence T. Drzal*

Department of Chemical Engineering and Materials Science, Composite Materials and Structures Center, Michigan State University, East Lansing, Michigan 48824, United States

Supporting Information

ABSTRACT: Exfoliated graphite nanoplatelets (GnP) has been investigated as an electrocatalyst support for fuel cell applications. GnP-supported Pt catalysts were synthesized by a microwave process in the presence of room temperature ionic liquids (RTILs). Thermal-oxidation resistance of GnP and GnP-supported Pt catalysts was studied by thermogravimetric analysis and compared with a variety of other carbon nanostructures: carbon black, graphite nanofiber, single- and multiwalled carbon nanotubes. GnP showed the best thermal-oxidative stability. The results obtained from X-ray diffraction, X-ray photoelectron spectroscopy, electrochemical testing, scanning and transmission electron microscopy showed that the RTIL synthesis method resulted in size reduction of Pt nanoparticle, improvement of Pt dispersion on GnP, and identification of the relationships between the mean size of Pt particles with increasing RTIL content. The interaction of Pt particles-GnP is stronger than that of a commercial Pt-CB, and the Pt/GnP catalysts prepared by this method have excellent electrocatalytic activity and stability for methanol oxidation.

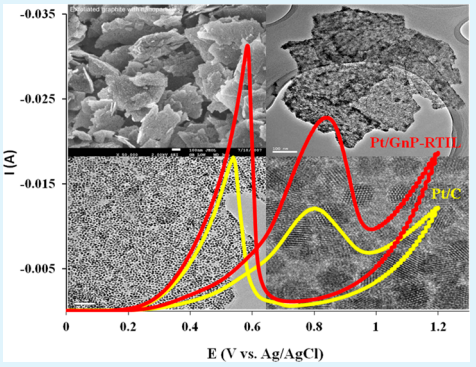

KEYWORDS: *exfoliated graphite nanoplatelet, room temperature ionic liquid, electrocatalyst, fuel cell, platinum nanoparticles*

1. INTRODUCTION

The proton exchange membrane fuel cell (PEMFC) is one of the promising alternative power sources for future energy security. Nanosized Pt-based particles are the most common catalysts used in PEMFC. The success of PEMFC depends considerably on cost, durability, and performance of the electrocatalyst in fuel cell stacks.[1] The high cost of electrocatalyst can be reduced by maximizing utilization of Pt catalysts on carbon supports which require properties such as high electrical conductivity, high surface area, excellent crystallinity, appropriate pore structure, and surface properties stable in a water generated environment.[2] The durability and long-term performance of these catalysts are predominantly affected by carbon corrosion which causes a decrease in the sites on carbon supports that are anchoring the Pt catalysts and thus results in catalyst detachment/aggregation and a structural collapse of the electrode in an extreme case. The development of highly active electrocatalysts dispersed on corrosion-resistant and inexpensive carbons is necessary for achieving the reliability of the PEMFC necessary for their widespread usage and reducing its total cost.

Conductive carbon black (CB) is currently widely used as a support for catalyst nanoparticles because of its easy availability and low cost. However, it has been shown that the presence of micropores and organo-sulfur groups on CB lead to a poor utilization and aggregation of catalyst nanoparticles, respectively.[3,4] In addition, thermochemical instability of CB under the operational condition of fuel cells causes the degradation of catalysts which limits fuel cell performance.[5] A variety of novel carbon nanostructures such as carbon nanotubes (CNT), graphite nanofiber (GNF), carbon nanohorns, and carbon nanocoil have been investigated.[6−11] Among them, CNT appears to be one of the most promising alternative supports due to excellent intrinsic properties such as high surface area, high chemical stability, and superior thermal, mechanical, and electrical properties.[12,13] Pt catalysts deposited on CNT showed improved corrosion-resistance due to the better stability of CNT and the better interaction between Pt particles and CNT than conventional CB support. Catalyst nanoparticles dispersed on the external walls of CNT have an additional advantage of reactant accessibility compared to those where the catalyst is located in the pores of the carbons. However, the high cost of CNT is still a barrier hindering their commercialization and special care is required for Pt catalyst deposition as well as the synthesis of ink with a good dispersion.

Graphene has been suggested as a catalyst support because it has a high electron in-plane transport rate and is potentially a low cost carbon in comparison with CNT.[14−17] Graphene studied as a support were mostly in the form of chemically reduced graphite oxide (rGO) or functionalized graphene sheets (FGS) thermally exfoliated over 1000 °C under an Ar

Received: March 3, 2014
Accepted: July 1, 2014
Published: July 1, 2014

environment. This alternative synthesis method is not attractive since the process for GO production consists of time-consuming multiple steps and requires hazardous strong oxidizing agents. GO has been found to be a "defective" graphene because it is wrinkled and full of holes or small defects caused by severe oxidation and is nonconductive. GO needs to be reduced to conductive graphene for real applications. The reduction can be accomplished with the help of a strong reducing agent or at high temperature to produce rGO and FGS. These graphenes have still damaged basal planes and a significant decrease of graphene surface area due to uncontrollable reaggregation. Low cost production of rGO and FGS does not appear to be a viable technology at this time.

GnP produced by expanding graphite intercalated compounds via thermal shock followed by pulverization consists of layers of graphene sheets. GnP is commercially available and thus much more cost-effective than rGO and FGS. GnP meets the key properties (e.g., high surface area, excellent mechanical strength, thermal and electrical conductivity) required to be an excellent carbon support and has a well-preserved highly ordered graphitic surface structure that is critical to excellent Pt/GnP catalyst durability. The presence of highly graphitic features decreases defect sites on its basal plane and edge site and increases π sites which act as anchoring sites of catalysts, enhancing the interaction between metal and carbon support and consequently suppressing the growth of catalyst particles, while the presence of oxygen functional groups can diminish metal−support interaction.[18] As a result, catalyst nanoparticles are well dispersed on the surface of GnP where they can make easy contact with the reactant. In spite of such potential benefits, the application of GnP as a carbon support for fuel cell catalysts has been identified in only a few reports.[19−21] This is due to the main difficulty in depositing catalyst nanoparticles on highly hydrophobic GnP with a high degree of intrinsic graphitization. Hence, it is required to modify GnP surface with either chemical oxidation or introduction of small molecules such as polyelectrolyte and surfactants prior to direct deposition of metal particles onto GnP. Compared with Pt/GnP, GO is a starting material in most cases of Pt/graphene catalysts. GO has very high surface area in the wet state and abundant oxygen functional groups on its basal and edge surface. Thus, GO itself has good interaction with Pt precursors and thus facilitate the synthesis of Pt/graphene without any pretreatment.

There are several advantageous features of room temperature ionic liquid (RTIL) in the synthesis of supported metal nanoparticles:[22,23] (1) the high polarity of RTIL can dissolve a variety of metal precursors, (2) the RTIL low surface tension can preferentially adsorb onto other surfaces and thus contribute to weakening the particle coarsening in the growth state of metallic particles leading to the generation of very small particles, (3) the high thermal stability of RTILs allows the reactions even at a high temperature, and (4) the excellent microwave (MW) absorption capability of RTILs assists in accelerating the heating rate of the solution in the MW process and thus promotes the production of fine metal nanoparticles by rapid nucleation rate of inorganic species. All of these advantages synergistically act to generate well dispersed small Pt particles on support materials.

In this paper, we report a simple technique to prepare GnP-supported Pt nanoparticles without any pretreatment of GnP with acids or small molecules to induce interaction between GnP and Pt precursor and to control the size of Pt particles deposited on GnP. This method is the result of a process for the reduction of Pt precursor in polyol solution in the presence of RTIL via MW heating. This research and fundamental characterization was carried out to determine the optimum particle size and dispersion and to estimate the interaction between Pt and GnP. Cyclic voltammetry measurements for GnP supported Pt catalysts were also performed to evaluate their catalytic activity.

2. EXPERIMENTAL SECTION

2.1. Materials and Catalyst Synthesis. Chloroplatinic acid hexahydrate ($H_2PtCl_6{\cdot}6H_2O$) purchased from Aldrich was used as a Pt precursor. Ethylene glycol (EG) from J.T. Baker was used as a reducing agent. Two different RTILs, 1-butyl-3-methylimidazolium hexafluorophosphate ($bmimPF_6$) and 1-butyl-3-methylimidazolium acetate ($bmimCH_3CO_2$) were obtained from Aldrich. $bmimPF_6$ is denoted as **RTIL-1** and $bmimCH_3CO_2$ as **RTIL-2** for convenience. GnP for this study was produced by expanding the graphite layers from acid-intercalated natural graphite via a MW heating and reducing the size of the expanded layers through an ultrasonication and milling process. Figure 1 shows the typical dimension of GnP with an average

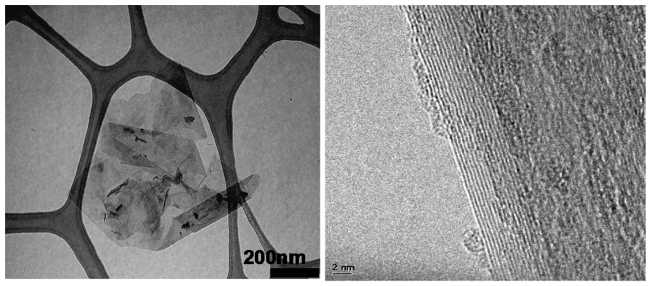

(a) (b)

Figure 1. Typical TEM pictures of GnP at (a) low and (b) high magnification.

thickness and diameter of approximately 8−10 nm and 1 μm, respectively. Single walled carbon nanotube (SWNT), multiwalled carbon nanotube (MWNT), carbon black (CB, Vulcan XC-72R), and GNF were purchased or provided from Cheap Tubes Inc., Aldrich, Cabot Co., and Nanomirae Inc., respectively, and used for the comparison of thermal-oxidative stability.

For the fabrication of Pt/GnP catalysts with 20 wt % Pt loading in the absence of RTIL, GnP was ultrasonically dispersed in 20 mL of EG for 30 min and a predetermined quantity of the Pt precursor dissolved in 2 mL of the reducing solvent separately was added to the solvent containing GnP. The mixture was mechanically mixed for 10 min, transferred into a commercial microwave oven, and irradiated under air for 60 s to reduce the Pt precursor. The resulting suspension was centrifuged and washed with an excess of acetone at least 5 times and dried in a vacuum oven at 373 K overnight. The catalyst obtained in this way is called the **Pt/GnP-N**. For Pt/GnP catalysts synthesized in the presence of the **RTIL-1** and **RTIL-2**, GnP was ultrasonically dispersed in EG for 30 min and, separately, a predetermined amount of the Pt precursor for 20 wt % Pt loading was added to EG and completely dissolved. They were mechanically mixed in a beaker for at least 30 min. Various contents of RTIL predissolved in EG various were added to the mixture, followed within 5 min by MW reduction in a MW oven for 60 s. The different molar ratios of RTIL/Pt precursor (RTIL/Pt = 0, 2.5, 5, 10, 50) were introduced. Other steps were the same as for the Pt/GnP-N catalyst. The Pt/GnP catalysts synthesized with the addition of $bmimPF_6$ and $bmimCH_3CO_2$ are denoted as **Pt/GnP-RTIL-1** and **Pt/GnP-RTIL-2**, respectively.

2.2. Characterization. The Pt particle formation process with Pt precursor of 1.5×10^{-5} M in EG was studied with UV−vis with a

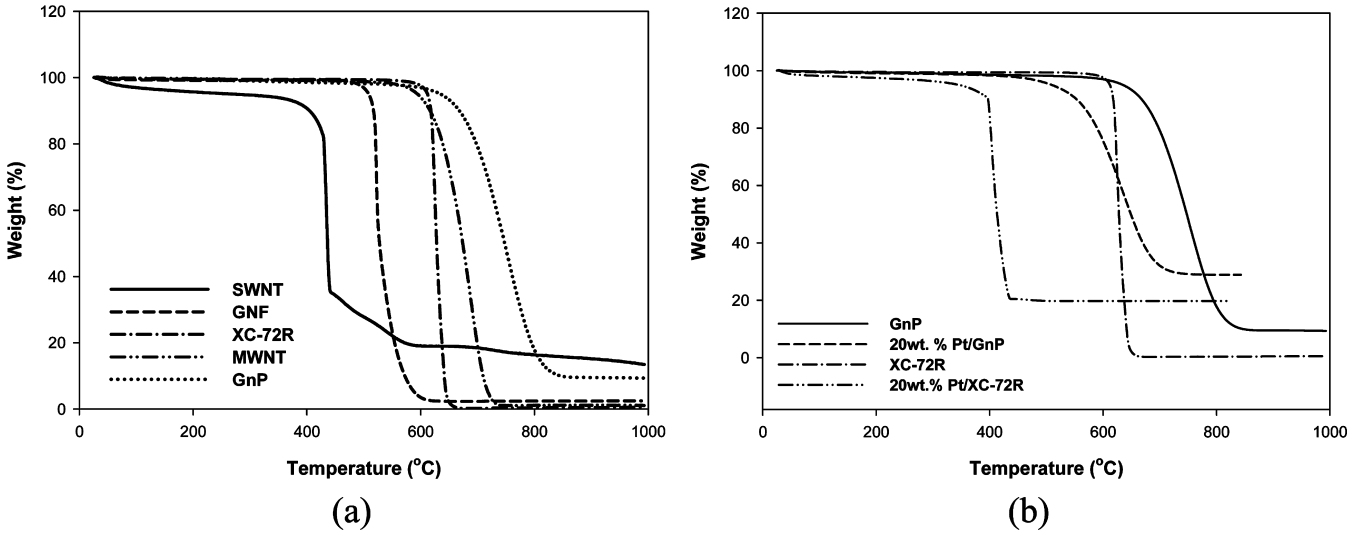

Figure 2. TGA curves of (a) various carbon supports and (b) the comparison of GnP and XC-72R decorated with and without 20 wt % Pt.

PerkinElmer Lamda 900 spectrometer over the range of 220−700 nm with 1 cm path length quartz cuvette. Pt catalysts dispersed on GnP were characterized by recording their X-ray diffraction (XRD) patterns on a Regaku Rotaflex 200B X-ray diffractometer using Cu-K_α radiation with a curved graphite monochromator. This was done to identify the phases present in the catalyst and to evaluate the lattice parameter and the particle size of the Pt crystallites dispersed on GnP. The 2θ region between 10° and 100° was scanned at 45 keV and 100 mV at a scan rate of 5°/min. Scanning electron microscopy (SEM) images were obtained on a JEOL 6300F for the general information on Pt dispersion on GnP. A transmission electron microscopy (TEM) investigation was also carried out with JEOL 100CX and JEOL 2200FS operating at a voltage of 100 and 200 keV for the morphology of the dispersed Pt nanoparticles and the determination of the average size of Pt particles. Thermogravimetric analysis (TGA 2950, TA Instruments) was performed to evaluate the degradation of GnP supported Pt catalysts and determine the Pt loading. Samples weighing 3−4 mg were tested over a temperature range from room temperature to 800 °C (for supported Pt catalysts) or 1000 °C (carbons) at 20 °C/min under flowing air. X-ray photoelectron spectroscopy (XPS) results of Pt/GnP catalysts were obtained with a Physical Electronics PHI 5400 ESCA system and used to investigate the presence of the oxide phases and the interaction between Pt and GnP. The Pt 4f region in the XPS spectrum was deconvoluted to indentify different metallic and oxidation states of Pt on the GnP.

An electrochemical investigation was performed by cyclic voltammetry (CV) using a potentiostat (Gamry Intstruments Inc., FAS2 Femtostat). Data was collected by Echem Analyst, which is software that was provided by the company. A conventional three-electrode cell equipped with a platinum wire counter electrode, an Ag/AgCl reference electrode, and a glassy carbon working electrode was used. The glassy carbon electrode with a 3 mm diameter was polished with a 0.05 μm alumina suspension before each experiment. The catalyst ink was prepared by ultrasonically dispersing 5 mg of Pt/GnP catalysts in 0.8 mL of alcohol, containing 0.1 mL of 0.1 wt % Nafion solution for 20 min. Then 20 μL of the catalyst ink was micropipetted on the top surface of the glassy carbon electrode. The CV experiments were performed in 1 M H_2SO_4 solution in the absence and the presence of 2 M CH_3OH at the scan rate of 50 mV/s. N_2 gas was purged for 15 min before starting the experiment. The chronoamperometry tests were also performed in 2 M CH_3OH/1 M H_2SO_4 at 0.45 V for the period of 3000 s to study the catalyst stability.

3. RESULTS AND DISCUSSION

3.1. Comparison of Various Carbon Supports. Supported electrocatalysts used in the fuel cells have to meet severe performance requirements for long-term fuel cell operation of over 40 000 h. Oxygen is supplied on the cathode side for the oxygen reduction reaction (ORR), and water generated in ORR has to be rapidly removed from the electrode. This environment has the potential for unwanted surface oxidation of carbon supports on the cathode. Support corrosion may occur due to the presence of oxygen, which is responsible for the performance loss of fuel cells. Therefore, the carbon support inevitably influences the catalytic activity of carbon supported catalysts in ORR at the fuel cell cathode.[24] Good corrosion or oxidation resistance is one of the important characteristics that an ideal support should possess for applications in fuel cells under strong oxidizing conditions. The high stabilization of the support toward corrosion can be accomplished by graphitizing carbon supports at very high temperature (e.g., >2000 °C) to reduce active surface sites like oxygen groups which are responsible for carbon corrosion in the fuel cell.[1] Thus, thermal-oxidative decomposition resistance may impart long-term stability to catalysts in acidic environments in energy generation/storage device operation because highly graphitized carbons are normally decomposed at higher temperature than less graphitized ones.

TGA analyses were used in order to compare thermal-oxidative resistance of various carbon supports and supported Pt electrocatalysts. According to Figure 2a, three carbons, MWNT, XC-72R, and GnP, started to decompose above 600 °C, while SWNT and GNF were completely decomposed before reaching 600 °C. The presence of metallic catalysts may be responsible for the fast decomposition of SWNT at low temperature. Thus, MWNT, CB (XC-72R), and GnP appeared to be more appropriate supports than SWNT and GNF on the basis of long-term stability in the corrosive environment in the fuel cell. GnP showed the highest thermal-oxidation resistance among all of the carbons, suggesting GnP can be a very promising durable catalyst support. This is as expected because the GnP basal plane surface has a high degree of graphitization and low concentration of defect sites, which provides a high concentration of π sites. The π sites on carbon act as anchoring sites for the Pt particles and are responsible for strong adsorption of Pt on carbon.[18]

It is also interesting to compare the combustion resistance of carbons loaded with the Pt particles because Pt on carbons can

act as catalysts accelerating chemical combustion of the carbon support which causes a decrease of fuel cell stability. The combustion stability of GnP and CB loaded with 20 wt % Pt particles is compared in Figure 2b. CB was selected because it is one of the carbon blacks most widely used at present with relatively excellent decomposition resistance as proven in Figure 2a. When both catalysts were exposed to air at an elevated temperature, CB lost its weight more rapidly at about 230 °C lower temperature than the bare CB. However, the decomposition temperature of GnP loaded with Pt particles shifted much less, only about 100 °C lower temperature compared to bare GnP. This result supports the excellence of GnP as a support stabilizing Pt electrocatalyst in an oxidizing environment.

3.2. Effect of RTIL on Synthesis and Characteristics of Pt/GnP. The size and dispersion of metal particles on GnP relies on when RTIL is introduced. Figure 3 briefly shows the

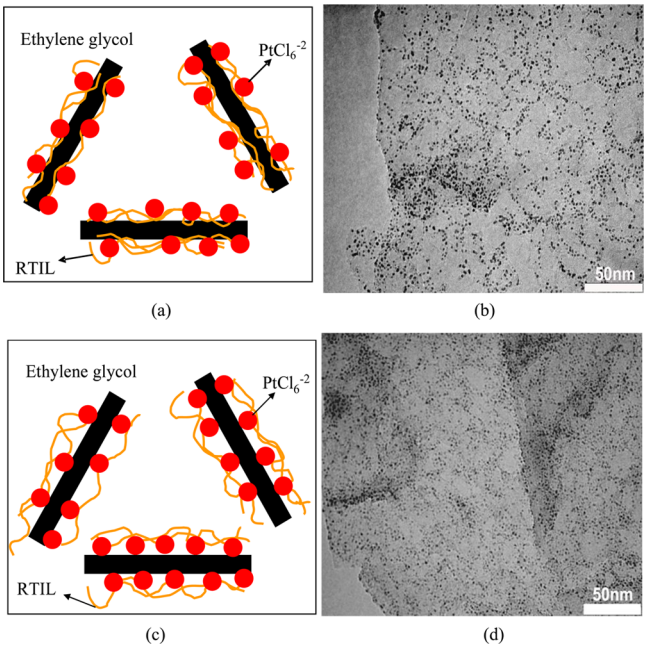

Figure 3. Suggested RTIL locations and TEM morphology of Pt/GnP-RTIL-2 sample when RTIL is added (a, b) before and (c, d) after the addition of Pt precursor.

schematic of the RTIL location in a solution containing platinum ions and TEM morphologies of the samples prepared by changing the sequence of RTIL addition to the EG solution containing GnP and Pt precursor. When RTIL is introduced in EG-GnP solution prior to the addition of Pt precursor (**Sequence-A**), it adsorbs onto the surface of GnP and thus metal ions interact weakly with GnP through the adsorbed layer of RTIL (Figure 3a). Hence, there is a possibility of the formation of some metal atoms and particles separate from the GnP surface, which leads to a decreasing number of Pt nanoparticles on GnP. If RTIL is added in EG-GnP solutions after the addition of Pt precursor (**Sequence-B**), Pt ions directly interact with the π sites on the xGnP basal plane and some oxygen groups at the GnP edge area (Figure 3c). RTIL may adsorb on the surface of metal ions or the GnP surface unoccupied by metal ions. Therefore, more metal atoms or particles form on the surface of GnP. TEM results shown in Figure 3b,d support such assumptions well. The sample prepared from **Sequence-B** has more particles on GnP than that from **Sequence-A.** However, the size of Pt particles was not affected in both cases.

FTIR analysis of Pt/GnP-RTIL-2 was performed to confirm the above hypothesis. As in the plots of Figure 4, the sample for

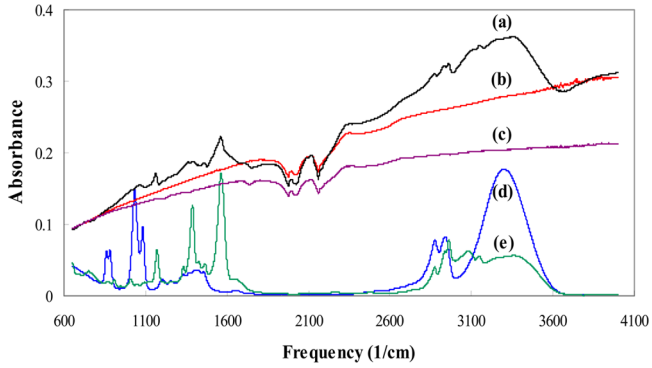

Figure 4. FTIR of (a) Pt/GnP-RTIL-2 (the addition of RTIL-2 prior to Pt precursor), (b) GnP, (c) Pt/xGnP-RTIL-2 (the addition of Pt precursor prior to bmimCH_3CO_2) (d) EG, and (e) RTIL-2.

Sequence-B has the same peak features as GnP (Figure 4b,c), indicating that RTIL was weekly adsorbed onto GnP and Pt and thus RTIL can be removed with ease after mild-washing with acetone. Meanwhile, in the case of **Sequence-A**, the sample shows peaks similar to those of RTIL (Figure 4a,c), suggesting that RTIL molecules strongly adsorb onto the surface of GnP and Pt. Thus, considerable traces of RTIL still remain on GnP after mild washing. In this sequence, too much RTIL may be detrimental to achieve the targeted metal loading because it blocks direct interaction between metal ions and GnP.

The effect of RTIL content on the process of Pt particle formation was investigated. The concentration of RTIL-2 was varied so that the molar ratio of RTIL-2 to Pt precursor was either 1, 5, 10, or 20. Figure 5a shows the UV−vis absorption spectra obtained after 10 s MW reduction and the effect of RTIL content on the reduction rate. The peak at 267 nm quickly decreased with increasing RTIL-2 content. When the molar ratio of RTIL-2/Pt precursor > 10, the peak completely disappeared even after 10 s MW heating. The absorption spectra above RTIL-2/Pt precursor = 20 were not affected in spite of the further increase of RTIL-2 concentration. This suggests that further addition of RTIL-2 is not needed to increase the reduction rate of Pt ions under the MW irradiation conditions.

UV−vis spectroscopy measurements were conducted to compare the reduction rate of $[PtCl_6]^{2-}$ in the presence of RTIL-1 and RTIL-2, and the results are compared in Figure 5b. The molar ratio between RTIL and Pt salt was 20. The resulting data were recorded after 10 s of MW irradiation. The peak height of Pt ions rapidly decreased in the presence of RTIL at a given MW time. RTIL-2 showed faster reduction of the peak height than RTIL-1, which results from the different polarity of the two RTILs because the reaction has been conducted in a microwave oven. Those two RTILs have the same cation, 1-butyl-3-methylimidazolium, but different anions. Only a difference in the polarity comes from anion groups. RTIL-2 is expected to have the higher polarity due to unsymmetrical arrangement by oxygen atoms than bmimPF_6 with fairly symmetrical molecular geometry. Hence, the

dx.doi.org/10.1021/am5012832 | ACS Appl. Mater. Interfaces 2014, 6, 12126−12136

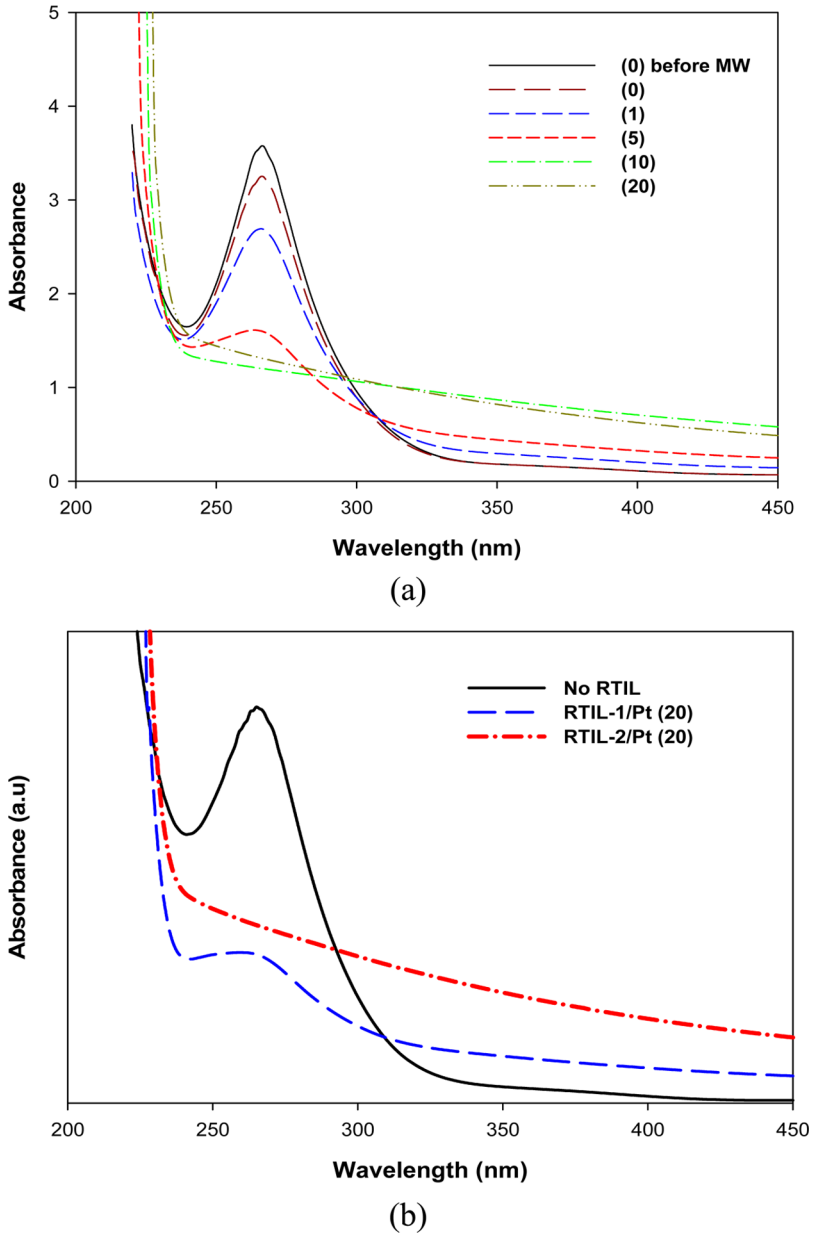

Figure 5. UV−vis absorption spectra obtained (a) in the presence of RTIL-2 at various concentrations and (b) in RTIL-1 and RTIL-2 at fixed concentration after 10 s MW reduction (numbers in parentheses represent molar ratio between RTIL and Pt precursor).

decrease of the peak intensity was more dramatic in the presence of RTIL-2 than RTIL-1, which enables to anticipate that RTIL-2 will produce the smaller Pt nanoparticles than RTIL-1 due to the faster reduction induced by the presence of RTIL-2. TEM analysis supports this result. A detailed explanation on the role of RTIL in producing metal nanoparticles and controlling their size and dispersion is available elsewhere.[25]

Figure 6 shows the XRD patterns measured on microwave-synthesized **Pt/GnP-N** and **Pt/GnP-RTIL-2** with the addition of various molar ratio of RTIL-2/Pt salt. The peaks at about 2θ = 26.58° and 54.6° are attributed to the graphite structure (002) and (004) of GnP, respectively. For Pt particles, the XRD pattern displays diffraction characteristic of a face-centered cubic crystal structure with major peaks at 2θ = 39.74° (111), 46.32° (200), 67.6° (220), and 81.62° (311). The diffraction peak at 2θ = 39.74° for Pt (111) corresponds to the *d*-spacing = 0.227 nm for the Pt (111) plane. While the sharp reflections are found at a low molar ratio of RTIL-2/Pt, the four characteristic peaks become broader at RTIL-2/Pt = 10 and disappear at RTIL-2/Pt = 50. This peak broadening suggests the formation of very small Pt particles and their good dispersion.[26] XRD implies that the average size of Pt particles decreases as the concentration of the RTIL-2 increases and visible evidence is in the TEM analysis.

TEM morphologies of Pt/GnP-RTIL prepared at RTIL/Pt = 50 were compared with Pt/GnP-N in Figure 7. While Pt particles with an average diameter of 3.74 nm were obtained in the absence of RTIL (Figure 7a), the mean size of Pt reduced to about 2.0 nm when RTIL-1 was introduced to the synthesis process (Figure 7b) and further decreased to about 1.68 nm when RTIL-2 was added (Figure 3d). The size distribution and dispersion of Pt particles were also drastically improved by the introduction of RTIL-1 and RTIL-2 (Figure 7c). The smaller Pt

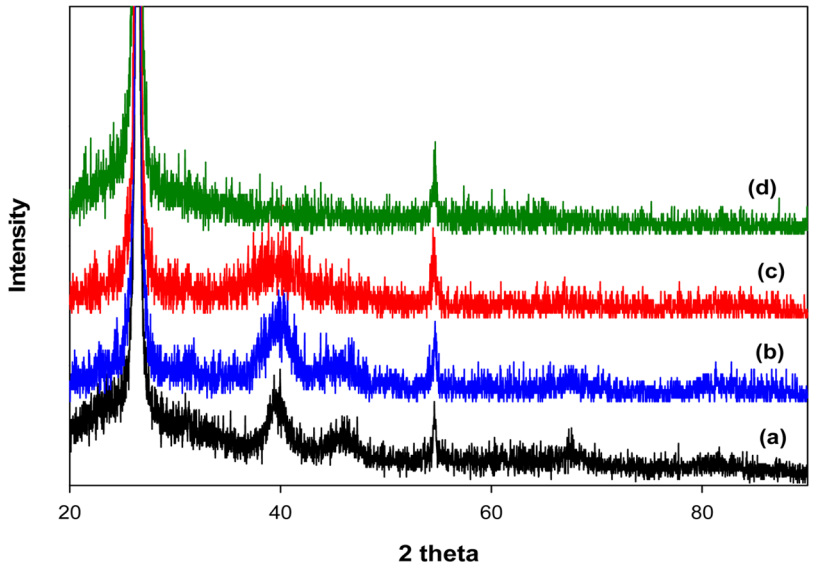

Figure 6. X-ray diffraction patterns of (a) Pt/GnP-N and Pt/GnP-RTIL-2 prepared with the addition of RTIL/Pt precursor = (b) 5, (c) 10, and (d) 50.

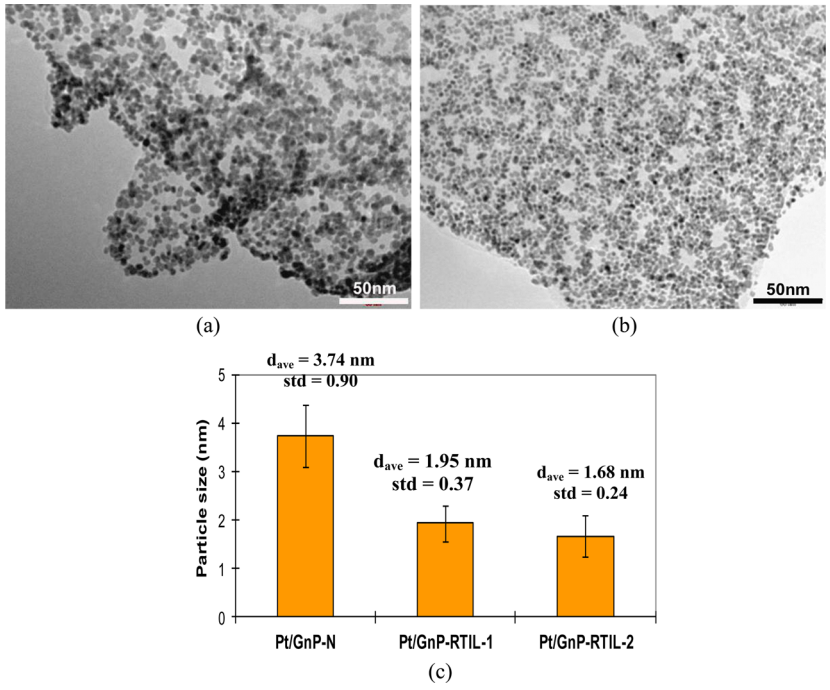

Figure 7. TEM images of (a) Pt/GnP-N, (b) Pt/GnP-RTIL-1, and (c) the mean size and size distribution of Pt particles in those Pt/GnP samples (Figure 3d is the TEM image of Pt/GnP-RTIL-2 synthesized at the same RTIL/Pt ratio).

particles generated by the addition of RTIL-2 are in good agreement with UV−vis spectroscopy analysis which proved RTIL-2 increased the reduction rate of the Pt precursor more rapidly than RTIL-1. The relatively high resolution TEM images provide further information on the Pt structure dispersed on GnP (Figure S1a in the Supporting Information). The lattice fringes are consistent with the well-developed metallic Pt crystallites. SEM image of dried Pt/GnP catalysts synthesized in the presence of a RTIL-1 is indicative of good dispersion of Pt catalysts not only on a single GnP but also on all of the GnP particles (Figure S1b in the Supporting Information). Additionally, the presence of RTIL contributes to the formation of much smaller Pt nanoparticles with a narrow size distribution compared to when RTIL is not present even in the case of the synthesis of highly loaded Pt catalysts on GnP (Figure S1c in the Supporting Information). Agglomerates of Pt particles were also rarely found for Pt/GnP-RTIL in spite of high loading metals (Figure S1d in the Supporting Information). All results suggest this synthetic method is a facile way of producing smaller Pt particles as well as controlling their size and dispersion regardless of Pt loading on GnP. This method can also be applied for the synthesis of various monometallic and bimetallic particles well-dispersed on GnP (Figure S2 in the Supporting Information).

Figure 8 displays the effect of RTIL content on the particle size and distribution of Pt particles. The addition of both RTIL-

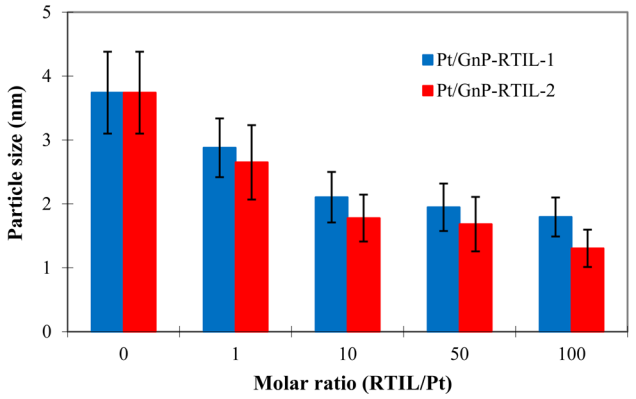

Figure 8. Effect of RTIL content on the size of Pt particles supported on GnP.

1 and RTIL-2 reduced the mean size of Pt particles and improved their size distribution. While Pt particles with a diameter of 3.74 nm and a large standard deviation were formed without any RTIL, the mean size of Pt particles was reduced below 3 nm and their size distribution became narrower when the RTILs corresponding to the molar ratio of RTILs/Pt precursor = 1 were present. The size of Pt particles further decreased with an increase of the RTIL content but asymptotically approached 1.5 nm beyond RTILs/Pt = 10 in molar ratio. Therefore, the RTILs content beyond RTILs/Pt = 10 does not seem to have a great effect on the further size reduction of Pt particles on GnP.

In Table 1, the averages sizes of the Pt particles in Pt/GnP catalysts prepared at different molar ratio of RTIL/Pt precursor

Table 1. Comparison of Morphological Data of XC-72R and GnP Supported Pt (20 wt %) Catalysts Prepared at Different Molar Ratios of RTIL/Pt

samples	RTIL/Pt	d_{TEM} (nm)	S (m^2/g)	D (%)
Pt/XC-72R		2.23 ± 0.55	125.7	48.4
Pt/GnP-N	0	3.74 ± 0.64	74.9	30.9
Pt/GnP-RTIL-1	2.5	2.88 ± 0.46	97.3	37.5
	5	2.54 ± 0.41	110.4	42.5
	10	2.10 ± 0.40	133.5	51.4
	50	1.95 ± 0.37	144.0	55.4
Pt/GnP-RTIL-2	2.5	2.64 ± 0.41	106.2	40.9
	5	2.01 ± 0.39	139.5	53.7
	10	1.78 ± 0.37	157.5	60.7
	50	1.68 ± 0.30	166.8	64.3

measured from TEM images were compared. The surface areas of those catalysts were calculated from the mean diameter of the particles obtained from the TEM images by using the following equation:

$$S = \frac{6000}{\rho d}$$

where S is the surface area (m^2/g), d the mean diameter of Pt particles (nm), and ρ the density of Pt (21.4 g/cm^3). The surface area of Pt/GnP-N was lower than the commercial Pt/XC-72R. However, the surface area of Pt/GnP-RTIL-1 and Pt/GnP-RTIL-2 was found to increase with the increasing molar ratio of RTIL/Pt and became higher than that of the commercial catalyst after RTIL/Pt reached a certain value. Dispersion (D) of the metal particles is an important parameter used to calculate the activity of the catalyst per surface metal atom. D is defined as the mean fraction of the total metal atoms exposed at the surface. D of Pt particles deposited on GnP roughly calculated from $d = 1.08/D$ (nm) using the TEM results.[27] The data showed that D can be increase as a result of the presence of both RTILs, but RTIL-2 is more effective in improving Pt dispersion on GnP than RTIL-1.

Pt/GnP catalysts prepared with and without the addition of RTIL-2 were analyzed by XPS to determine the oxidative state of Pt particles as well as the interaction between Pt and GnP. The Pt 4f signal in Pt/GnP-N consisting of three pairs of doublets (Figure S3 in the Supporting Information). The two strong energy bands at 71.66 and 74.99 eV are due to Pt particles in a metallic state, while two weak energy bands observed at 73.09 and 76.42 eV can be assigned to Pt^{2+} and Pt^{4+} in an oxidation state. The XPS study explains the electron donation by Pt to a carbon support.[28] The Pt $4f_{7/2}$ peak for the Pt/GnP catalyst shifted to higher values with respect to 71.1 eV for Pt metal in the literature, indicating the strong interaction between Pt and GnP through electron transfer from Pt to the surface of GnP.[29,30] This shift can be interpreted as a small particle effect as reported in refs 31 and 32. On the other hand, the complete reduction of Pt precursors with and without RTIL addition in a MW heating process supported the absence of a peak at 198 eV corresponding to Cl^- which is responsible for the catalytic loss or degradation of Pt/GnP catalysts (Figure S4 in the Supporting Information).

Deconvolution of the XPS spectrum was carried out for Pt/GnP catalysts prepared at different RTIL-2/Pt precursor molar ratios = 2.5, 5, 10, and 50. The percentage of Pt particles in metallic and oxidative states was calculated and is listed in Table 2. The results for unsupported Pt blacks synthesized in

Table 2. Peak Location of Pt 4f and Content of Different Pt Species Determined from Pt/GnP-N and Pt/GnP-RTIL-2 Samples

samples	RTIL/Pt	metallic Pt (peak location, eV)	Pt oxide (peak location, eV)
Pt black		64.6% (71.38, 74.72)	35.4% (72.52, 75.96)
Pt-RTIL-2	2.5	65.8% (70.67, 74.03)	34.2% (71.60, 74.03)
	5	71.1% (71.09, 74.39)	28.9% (72.17, 74.39)
	50	73.6% (70.54, 73.87)	26.4% (71.67, 75.50)
Pt/XC-72R		65.5% (71.78, 75.10)	34.4% (73.35, 76.91)
Pt/GnP-N		65.5% (71.66, 74.99)	34.5% (73.09, 76.42)
Pt/GnP-RTIL-2	2.5	82.7% (71.83, 75.16)	17.3% (73.40, 76.73)
	5	73.8% (71.96, 75.29)	26.2% (73.45, 76.78)
	10	72.4% (72.17, 75.50)	27.6% (73.40, 76.73)
	50	67.8% (72.12, 75.45)	32.2% (73.60, 76.93)

the absence and the presence of RTIL-2 and a commercial Pt/XC-72R. were also included for comparison. While Pt/GnP-N and Pt/XC-72R catalyst showed similar content of metallic Pt particles, higher percentages of metallic Pt were present in Pt/GnP-RTIL-2. However, the content of metallic Pt species decreased with an increase of RTIL-2 content. It is not clear if the partial oxidation of Pt takes place in the middle of the synthesis process for producing supported catalysts and/or if the reduction reaction of the Pt precursor is incomplete. Pt oxidation can occur when the supported Pt is exposed to air because oxygen can easily be chemisorbed on the surface of the Pt clusters. The presence of Pt oxides may be responsible for the detection of oxygen-containing species found on the oxygen

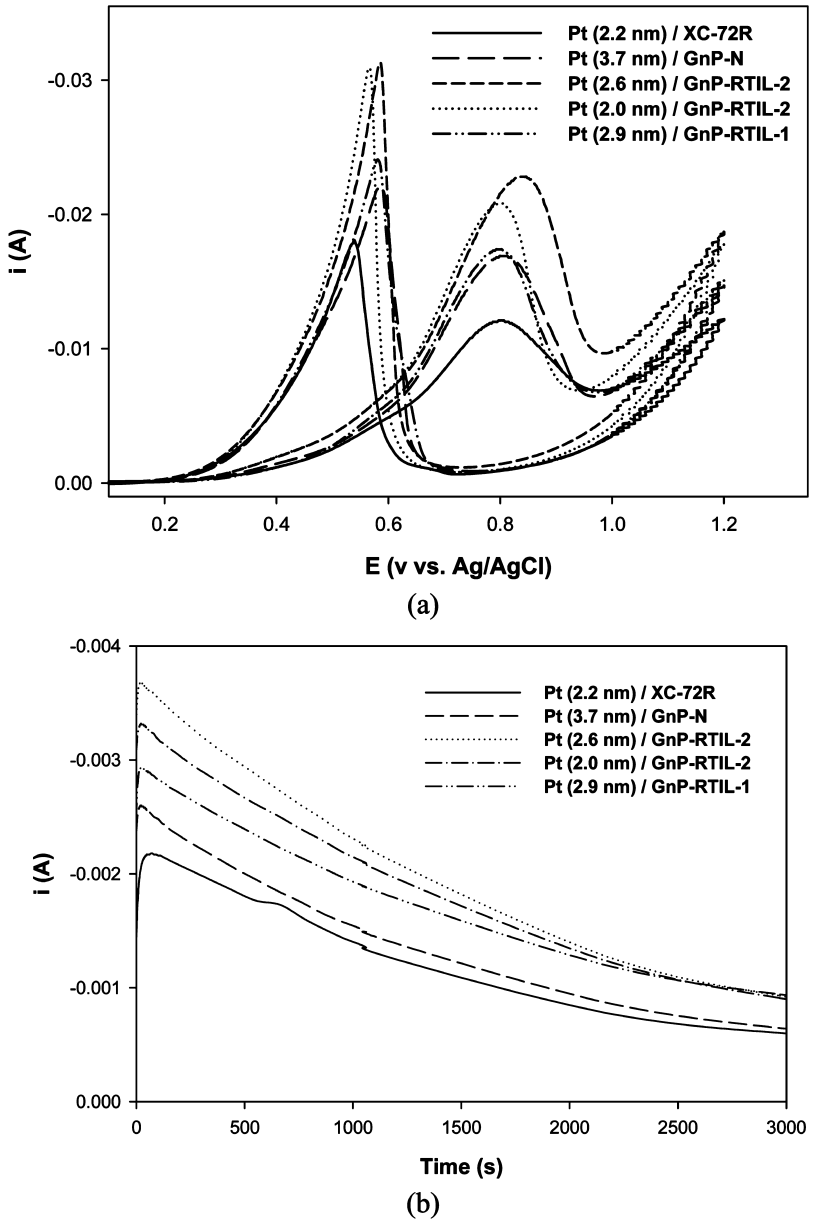

Figure 9. (a) Comparison of catalytic activity and (b) chronoamperometry curves for methanol oxidation at 0.45 V on Pt/XC-72R, Pt/GnP-N, Pt/GnP- RTIL-1, and Pt/GnP- RTIL-2 catalysts.

groups of the GnP support. The reduction of Pt species content in oxidation is possibly due to the lower susceptibility to oxidation of the Pt nanoparticles, which adsorb RTIL-2. However, the decrease of metallic Pt at high molar catalysts may result from the increase of RTIL-2 on Pt particles. On the other hand, the electronic interaction between Pt and GnP can be recognized by the shift of metallic Pt peak location for Pt/GnP with respect to unsupported Pt.[33] As listed in Table 2, the metallic Pt peaks for GnP-supported RTIL-2/Pt precursor molar ratio = 0, 2.5, 5, and 50, catalysts shifted to higher values by 0.28, 1.16, 0.87, and 1.68 eV with respect to corresponding unsupported Pt blacks (71.1 eV). This result can be interpreted as related to the presence of the Pt-GnP electronic effect. The Pt-GnP interaction was through an electron transfer from Pt to the surface of GnP.[18,34] It is not likely that mechanical interlocking is responsible for the adhesion of the Pt nanoparticles to the GnP. Adhesion most likely arises from molecular, electrostatic, and/or chemical surface forces acting across the interface of two solids.[35] The shift of Pt peaks for Pt/GnP-RTIL-2 samples was larger than for the commercial Pt/XC-72R, indicating that the interaction between Pt-GnP is stronger than that between Pt-XC-72R. The small size effect is excluded because the Pt size for supported samples is similar to that for corresponding unsupported particles.

3.3. Electrocatalytic Activity. The electrochemical performance of Pt/GnP catalysts synthesized in the absence and the presence of RTIL-1 and RTIL-2 was studied for methanol oxidation in 1 M H_2SO_4 + 2 M CH_3OH solution at 50 mV/s scan rate at the room temperature. A commercial Pt/XC-72R catalyst was also tested for comparison. All of the catalysts have approximately 20 wt % of Pt particles, which was determined by TGA. Figure 9a shows the results of cyclic voltammetry measurements for Pt/GnP and Pt/XC-72R catalysts. The peaks in the current at around 0.8 V in the forward scan and at around 0.57 V in the reverse scan represented the methanol oxidation and the removal of the residual carbon species

Table 3. Mass Activity of Pt Particles for Pt/GnP Catalyst Prepared via Microwave Irradiation at the Various Molar Ratios of RTIL/Pt

samples	Pt size (nm)	Pt loading (wt %)[a]	mass of Pt (mg)	mass activity at peak in forward (mA/mg Pt)	mass activity at peak in reverse (mA/mg Pt)
Pt/XC-72R	2.2	19.8	0.0218	577	828
Pt/GnP-N	3.7	19.7	0.0217	788	1025
Pt/GnP-RTIL-1	2.9	19.6	0.0215	840	1135
Pt/GnP-RTIL-2	2.6	19.4	0.0213	1090	1485
Pt/GnP-RTIL-2	2.0	18.9	0.0208	999	1487

[a]Measured from TGA in an air environment at 25 °C/min ramp rate.

formed in the forward scan.[36,37] All of the Pt/GnP catalysts showed higher oxidation current than Pt/XC-72R, indicating that the former are more active for methanol oxidation than the latter. The oxidation current obtained from Pt/GnP-RTIL-2 catalysts increased almost twice as much as the Pt/XC-72R. This enhancement of the catalytic activity for methanol oxidation may be attributed to the improved utilization of the Pt phase on the surface of GnP. This better Pt dispersion and utilization on the Pt/GnP catalysts were due to the larger and highly accessible surface area provided by the formation of the Pt nanoparticles on the surface of GnP. Pt particles on XC-72R can be trapped in its pores where the reactant cannot access and Nafion cannot form a three phase boundary but there may be no such Pt regions on GnP.[38] This difference may explain the efficiency of Pt/GnP catalysts over the commercial catalyst. The stronger interaction between Pt particles and GnP may be another possible reason for explaining the better catalytic performance of Pt/GnP-RTIL-2, which was proved by data from XPS spectra of Pt 4f. The ratio between peak currents in the forward (I_f) and reverse (I_b) scans is used to evaluate the tolerance of electrocatalysts in methanol oxidation.[39] A high I_f/I_b implies better CO-tolerance. The values of I_f/I_b calculated from cyclic voltammograns in Figure 9a for all GnP-supported Pt were larger than that of Pt/XC-72R, indicating improved poison tolerance of Pt/GnP catalysts (Table S1 in the Supporting Information).

The catalytic stability is another important evaluation of carbon supported Pt catalysts for methanol oxidation. The current−time curves at 0.45 V are shown in Figure 9b. The initial methanol oxidation currents for Pt/GnP catalysts were higher than that of a commercial Pt/XC-72R and their order of the initial currents was in good agreement with the results of CV measurements. The current for all the catalysts gradually decayed with time, which is caused by the adsorption of CO_x species on the surface of Pt particles during the methanol oxidation reaction.[40] The current values for Pt/GnP catalysts synthesized in the presence of RTIL-1 and RTIL-2 were always greater than that of Pt/XC-72R for the period of the measurement, suggesting that the Pt/GnP-RTIL catalysts had better long-term stability than Pt/XC-72R.

Mass activity, the way to express the catalytic activity of Pt particles dispersed on carbon supports, is of particular importance because the cost of electrodes in fuel cells depends on the amount of Pt-based catalysts. If the catalysts have high mass activity, it is possible to reduce the loading of Pt. Mass activities of Pt/GnP catalysts calculated at peaks in the forward and the reverse scans were compared with those of Pt/XC-72R catalyst in Table 3. All of the Pt/GnP catalyst showed a greater activity than Pt/XC-72R and two different Pt/GnP-RTIL-2 samples with 2.64 and 2.01 nm of Pt produced a much higher mass activity than Pt/XC-72R with 2.23 nm Pt. They showed an 80% increase in mass activity compared to Pt/XC-72R, resulting from much better utilization of the Pt particles on GnP. It was reported in the literature that 3 nm Pt-based particles exhibited the highest mass catalytic activity for methanol oxidation and oxidation reduction.[41,42] However, that report does not agree with the present result. According to the result of mass activity, a more critical factor influencing catalytic activity of support Pt catalysts seemed to be the utilization of Pt particles rather than the Pt size. The structure of GnP that allows the active phase to make an easy contact with the reactant and the proton conductive materials simultaneously also contributed to the increase in the utilization of Pt phase in Pt/GnP catalysts.

4. CONCLUSION

The main purpose of this work is to report a simply way of depositing Pt nanoparticles and manipulating their size on very hydrophobic GnP and to investigate GnP as a support for the catalytic oxidation of methanol in DMFC. GnP has suitable properties such as good electronic conductivity, high corrosion resistance, high surface area, high mechanical properties, high accessible area for the reactant, as well as low resistance between the interface of electrolytes and GnP. The thermo-oxidative stability and combustion resistance of GnP have been studied with TGA and compared with other carbon nanostructures. TGA results proved that GnP has the highest stability among the other carbon candidates for fuel cell applications.

The 20 wt % Pt/GnP catalysts were prepared in the presence of various molar ratios of RTIL to chloroplatinic acid hexahydrate in EG as a reducing agent via microwave technique. TEM and XRD results reveal that, regardless of Pt loading level, highly dispersed Pt nanoparticles below 3 nm with a narrow size distribution were synthesized on the GnP by introducing RTIL to the solution. The size of Pt nanoparticles could be controlled by changing the molar ratio of RTIL/GnP.

Pt/GnP catalysts exhibit higher catalytic activity than the commercial Pt/XC-72R catalysts due to higher dispersion and utilization of the Pt particles as well as stronger Pt-support interaction. All the results indicate the use of GnP as a support has great potential not only for DMFC but also for other low temperature fuel cells.

■ ASSOCIATED CONTENT

Supporting Information

TEM images of various metal and metal alloy desposited on GnP, XPS spectra, and CV characterization of Pt/GnP catalysts synthesiszed in the presence of RTIL. This material is available free of charge via the Internet at http://pubs.acs.org.

AUTHOR INFORMATION

Corresponding Author

*E-mail: drzal@egr.msu.edu.

Present Address

[†]I.D.: XG Sciences, Inc., 3101 Grand Oak Drive, Lansing, MI 48911.

Author Contributions

I. Do designed and performed the experiments, analyzed the data, and wrote the paper. L. T. Drzal wrote and reviewed the paper. All authors approved the final manuscript.

Funding

Portions of this research were supported by Grant 06-1-P1-0425 "Low Cost, Multifuntional Nanomaterial Additive for Polymers and Composite Materials" from the State of Michigan Economic Development Corporation's 21st Century Jobs Fund.

Notes

The authors declare no competing financial interest.

ACKNOWLEDGMENTS

The authors would like to thank Dr. Stanley L. Flegler, Director of the Center for Advanced Microscopy in Michigan State University (MSU), for acquiring the SEM images of Pt/GnP catalysts listed in this work and Dr. Per Askeland at Composite Materials and Structures Center at MSU for his assistance with the XPS data.

REFERENCES

(1) He, C.; Desai, S.; Brown, G.; Bollepalli, S. PEM Fuel Cell Catalysts: Cost, Performance, and Durability. *Interface* **2005**, *14*, 41−44.

(2) Jha, N.; Leela Mohana Reddy, A.; Shaijumon, M. M.; Rajalakshmi, N.; Ramaprabhu, S. Pt−Ru/Multi-Walled Carbon Nanotubes as Electrocatalysts for Direct Methanol Fuel Cell. *Int. J. Hydrogen Energy* **2008**, *33*, 427−433.

(3) Antolini, E.; Gonzalez, E. R. Polymer Supports for Low-Temperature Fuel Cell Catalysts. *Appl. Catal., A* **2009**, *365*, 1−19.

(4) Roy, S. C.; Christiensen, P. A.; Hamnett, A.; Thomas, K. M.; Trapp, V. Direct Methanol Fuel Cell Cathodes with Sulfur and Nitrogen-Based Carbon Functionality. *J. Electrochem. Soc.* **1996**, *143*, 3073−3079.

(5) Shao, Y.; Yin, G.; Gao, Y. Understanding and Approaches for the Durability Issues of Pt-based Catalysts for PEM Fuel Cell. *J. Power Sources* **2007**, *171*, 558−566.

(6) Kongkanand, A.; Kuwabata, S.; Girishkumar, G.; Kamat, P. Single-Wall Carbon Nanotubes Supported Platinum Nanoparticles with Improved Electrocatalytic Activity for Oxygen Reduction Reaction. *Langmuir* **2006**, *22*, 2392−2396.

(7) Wu, G.; Chen, Y. S.; Xu, B. Q. Remarkable Support Effect of SWNTs in Pt Catalyst for Methanol Electrooxidation. *Electrochem. Commun.* **2005**, *7*, 1237−1243.

(8) Li, W.; Liang, C.; Zhou, W.; Qiu, J.; Zhou, Z. H.; Sun, G.; Xin, Q. Preparation and Characterization of Multiwalled Carbon Nanotube-Supported Platinum for Cathode Catalysts of Direct Methanol Fuel Cells. *J. Phys. Chem. B* **2003**, *107*, 6292−6299.

(9) Park, K.; Sung, Y.; Han, S.; Yun, Y.; Hyeon, T. Origin of the Enhanced Catalytic Activity of Carbon Nanocoil-Supported PtRu Alloy Electrocatalysts. *J. Phys. Chem. B* **2004**, *108*, 939−944.

(10) Gan, L.; Du, H.; Li, B.; Kang, F. Surface-Reconstructed Graphite Nanofibers as a Support for Cathode Catalysts of Fuel Cells. *Chem. Commun.* **2011**, *47*, 3900−3902.

(11) Yoshitake, T.; Shimakawa, Y.; Kuroshima, S.; Kimura, H.; Ichihashi, T.; Kubo, Y.; Kasuya, D.; Takahashi, K.; Kokai, F.; Yudasaka, M.; Iijima, S. Preparation of Fine Platinum Catalyst Supported on Single-Wall Carbon Nanohorns for Fuel Cell Application. *Phys. B: Condens. Matter* **2002**, *323*, 124−126.

(12) Solla-Gullon, J.; Lafuente, E.; Aldaz, A.; Martinez, M. T.; Feliu, J. M. Electrochemical Characterization and Reactivity of Pt Nanoparticles Supported on Single-Walled Carbon Nanotubes. *Electrochim. Acta* **2007**, *52*, 5582−5590.

(13) Dyke, C. A.; Tour, J. M. Covalent Functionalization of Single-Walled Carbon Nanotubes for Materials Applications. *J. Phys. Chem. A* **2004**, *108*, 11151−11159.

(14) Kou, R.; Shao, Y.; Wang, D.; Englehard, M. H.; Kwak, J. H.; Wang, J.; Viswanathan, V. V.; Wang, C.; Lin, Y.; Wang, Y.; Aksay, I. A.; Liu, J. Enhanced Activity and Stability of Pt Catalysts on Functionalized Graphene Sheets for Electrocatalytic Oxygen Reduction. *Electrochem. Commun.* **2009**, *11*, 954−957.

(15) Wang, L.; Tian, G.; Mu, G.; Zhang, H.; Fu, H. Facile Synthesis of Pt Nanocrystals/Graphene Composite with Excellent Methanol Electro-Oxidation Performance. *MRS Bull.* **2012**, *47*, 4311−4315.

(16) Li, Y.; Zhu, E.; McLouth, T.; Chiu, C. Y.; Huang, X.; Huang, Y. Stabilization of High-Performance Oxygen Reduction Reaction Pt Electrocatalyst Supported on Reduced Graphene Oxide/Carbon Black Composite. *J. Am. Chem. Soc.* **2012**, *134*, 12326−12329.

(17) Imran Jafri, R.; Arockiados, T.; Rajalakshmi, N.; Ramaprabhu, S. Nanostructured Pt Dispersed on Graphene-Multiwalled Carbon nanotube Hybrid Nanomaterials as Electrocatalyst for PEMFC. *J. Electrochem. Soc.* **2010**, *157*, B874−879.

(18) Yu, X.; Ye, S. Recent Advances in Activity and Durability Enhancement of Pt/C Catalytic Cathode in PEMFC Part I. Physico-Chemical and Electronic Interaction between Pt and Carbon Support, and Activity Enhancement of Pt/C Catalyst. *J. Power Sources* **2007**, *172*, 133−144.

(19) Lu, J.; Do, I.; Drzal, L. T.; Worden, R. M.; Lee, I. Nanometal-Decorated Exfoliated Graphite Nanoplatelet Based Glucose Biosensors with High Sensitivity and Fast Response. *ACS Nano* **2008**, *2*, 1825−1832.

(20) Shao, Y.; Zhang, S.; Wang, C.; Nie, Z.; Liu, J.; Wang, Y.; Lin, Y. Highly Durable Graphene Nanoplatelets Supported Pt Nanocatalysts for Oxygen Reduction. *J. Power Sources* **2010**, *195*, 4600−4605.

(21) Xia, G.; Huang, C.; Wang, Y. Highly Uniform Platinum Nanoparticles Supported on Graphite Nanoplatelets as a Catalyst for Proton Exchange Membrane Fuel Cells. *Int. J. Hydrogen Energy* **2013**, *38*, 13754−13761.

(22) Antonietti, M.; Kuang, D.; Smarsly, B.; Zhou, Y. Ionic Liquids for the Convenient Synthesis of Functional Nanoparticles and Other Inorganic Nanostructures. *Angew. Chem., Int. Ed.* **2004**, *43*, 4988−4992.

(23) Cai, R.; Sun, M.; Chen, Z.; Munoz, R.; O'Neill, C.; Beving, D.; Yan, Y. Ionothermal Synthesis of Oriented Zeolite AEL Films and Their Application as Corrosion-Resistant Coatings. *Angew. Chem., Int. Ed.* **2008**, *47*, 525−528.

(24) Bessel, C. A.; Laubernds, K.; Rodriguez, N. M.; Baker, R. T. K. Graphite Nanofibers as an Electrode for Fuel Cell Applications. *J. Phys. Chem. B* **2001**, *105*, 1115−1118.

(25) Do, I.; Drzal, L. T. Room Temperature Ionic Liquids for Size Control of Noble Metal Nanoparticles on Carbon Supports. *Carbon* **2014**, *75*, 43−45.

(26) Radmilovic, V.; Gasteiger, H. A.; Ross, P. N. Structure and Chemical Composition of a Supported Pt-Ru Electrocatalyst for Methanol Oxidation. *J. Catal.* **1995**, *154*, 98−106.

(27) Benson, J. E.; Boudart, J. Hydrogen-Oxygen Titration Method for the Measurement of Supported Platinum Surface Areas. *J. Catal.* **1965**, *4*, 704−710.

(28) Escard, J.; Leclerc, C.; Contour, J. P. The State of Supported Iridium in a Hydrazine Decomposition Catalyst. *J. Catal.* **1973**, *29*, 31−39.

(29) Antolini, E.; Giorgi, L.; Cardellini, F.; Passalacqua, E. Physical and Morphological Characteristics and Electrochemical Behaviour in PEM Fuel Cells of PtRu/C Catalysts. *J. Solid State Electrochem.* **2001**, *5*, 131−140.

(30) Shukla, A. K.; Ravikumar, M. K.; Roy, A.; Barman, S. R.; Sarma, D. D.; Arico, A. S.; Antonucci, V.; Pino, L.; Giordano, N. Electro-oxidation of Methanol in Sulfuric Acid Electrolyte on Plantinized-Carbon Electrodes with Several Functional-Group Characteristics. *J. Electrochem. Soc.* **1994**, *141* (6), 1517−1521.
(31) Mason, M. G. Electronic Structure of Supported Small Metal Clusters. *Phys. Rev. B* **1983**, *27*, 748−762.
(32) Eberhadt, W.; Fayet, P.; Cox, D. M.; Fu, Z.; Kaldor, A.; Sherwood, R.; Sondericker, D. Photoemission from Mass-Selected Monodispersed Pt Clusters. *Phys. Rev. Lett.* **1990**, *64*, 780−783.
(33) Antolini, E. Formation, Microstructural Characteristics and Stability of Carbon Supported Platinum Catalysts for Low Temperature Fuel Cells. *J. Mater. Sci.* **2003**, *38*, 2995−3005.
(34) Shukla, A. K.; Ravikumar, M. K.; Roy, A.; Barman, S. R.; Sarma, D. D.; Arico, A. S.; Antonucci, V.; Pino, L.; Giordano, N. Electro-oxidation of Methanol in Sulfuric Acid Electrolyte on Platinized-Carbon Electrodes with Several Functional-Group Characteristics. *J. Electrochem. Soc.* **1994**, *141*, 1517−1522.
(35) Mittal, K. L. Adhesion Aspects of Metallization of Organic Polymer Surfaces. *J. Vac. Sci. Technol.* **1976**, *13*, 19−25.
(36) Yajima, T.; Uchida, H.; Watanabe, M. In-Situ ATR-FTIR Spectroscopic Study of Electro-oxidation of Methanol and Adsorbed CO at Pt-Ru Alloy. *J. Phys. Chem. B* **2004**, *108*, 2654−2659.
(37) Lamy, C.; Belgsir, E. M.; Leger, J.-M. Electrocatalytic Oxidation of Aliphatic Alcohols: Application to the Direct Alcohol Fuel Cell (DAFC). *J. Appl. Electrochem.* **2001**, *31*, 799−809.
(38) Shao, Y.; Liu, J.; Wang, Y.; Lin, Y. Novel Catalysts Support Materials for PEM fuel cells: Current Status and Future Prospects. *J. Mater. Chem.* **2009**, *19*, 46−59.
(39) Xu, C.; Wang, L.; Wang, R.; Wang, K.; Zhang, Y.; Tian, F.; Ding, Y. Nanotubular Mesoporous Bimetallic Nanostructures with Enhanced Electrocatalytic Performance. *Adv. Mater.* **2009**, *21*, 2165−2169.
(40) Jiang, J.; Kucemak, A. Electrooxidation of Small Organic Molecules on Mesoporous Precious Metal Catalysts II: CO and Methanol on Platinum−Ruthenium Alloy. *J. Electroanal. Chem.* **2003**, *543*, 187−199.
(41) Kinoshita, K. Particle Size Effects for Oxygen Reduction on Highly Dispersed Platinum in Acid Electrolytes. *J. Electrochem. Soc.* **1990**, *137*, 845−848.
(42) Takasu, Y.; Itaya, H.; Iwazaki, T.; Miyoshi, R.; Ohmuna, T.; Susmoto, W. Size Effects of Ultrafine Pt−Ru Particles on the Electrocatalytic Oxidation of Methanol. *Chem. Commun.* **2001**, *4*, 341−342.